Research Article | Vol. 26, No. 5 | 5 Mar 2018 | OPTICS EXPRESS 6400
Optics EXPRESS

Nonlinearities in GaAs cavities with high CW input powers enabled by photo-oxidation quenching through ALD encapsulation

GREGORY MOILLE,[1,2] SYLVAIN COMBRIÉ,[2] LAURENCE MORGENROTH,[3] GAËLLE LEHOUCQ,[2] SÉBASTIEN SAUVAGE,[1] MOUSTAFA EL KURDI,[1] PHILIPPE BOUCAUD,[1] ALFREDO DE ROSSI,[2] AND XAVIER CHECOURY[1,*]

[1]*Centre de Nanosciences et de Nanotechnologies, CNRS, Univ. Paris-Sud, Université Paris-Saclay, C2N - Orsay, 91405 Orsay cedex, France*
[2]*Thales Research and Technology France, 1 avenue Augustin Fresnel, 91767 Palaiseau, France*
[3]*Institut d'Electronique de Microélectronique et de Nanotechnologies, 59652 Villeneuve d'Ascq, France*
[4] *Current address: Center for Nanoscale Science and Technology, National Institute of Standards and Technology, Gaithersburg, MD and Maryland Nanocenter, University of Maryland, College Park, MD 20742, USA*
[*]*xavier.checoury@u-psud.fr*

Abstract: We demonstrate that conformal encapsulation using atomic layer deposition of GaAs nano-cavity resonator made of photonic crystal cavity prevents photo-induced oxidation. This improvement allows injecting a large quantity of energy in the resonator without any degradation of the material, thus enabling spectral stability of the resonance. We prove second harmonic and third harmonic generation over more than one decade of pump power variation, thanks to this encapsulation, with a total efficiency ($\eta_{SHG} = 8.3 \times 10^{-5}$ W^{-1} and $\eta_{THG} = 1.2 \times 10^{-3}$ W^{-2}) and a large net output energy for both operations ($P^{out}_{SHG} = 0.2$ nW and $P^{out}_{THG} = 8$ pW).

OCIS codes: (230.5298) Photonic crystals; (130.5990) Semiconductors; (190.0190) Nonlinear optics

References and links

1. S. B. Papp, K. Beha, P. Del'Haye, F. Quinlan, H. Lee, K. J. Vahala, and S. A. Diddams, "Microresonator frequency comb optical clock," Optica **1**, 10–5 (2014).
2. T. Udem, R. Holzwarth, and T. W. Hansch, "Optical frequency metrology," Nature **416**, 233–237 (2002).
3. Y. Barad, M. Horowitz, and Y. Silberberg, "Third harmonic generation for nonlinear scanning laser microscopy," (SPIE, 1997).
4. Y. Zeng, I. Roland, X. Checoury, Z. Han, M. El Kurdi, S. Sauvage, B. Gayral, C. Brimont, T. Guillet, F. Semond, and P. Boucaud, "Imaging of Photonic Crystal Localized Modes through Third-Harmonic Generation," ACS Photonics (2016).
5. B. Corcoran, C. Monat, C. Grillet, D. J. Moss, B. J. Eggleton, T. White, L. O'Faolain, and T. F. Krauss, "Green light emission in silicon through slow-light enhanced third-harmonic generation in photonic-crystal waveguides," Nat. Photonics **3**, 206–210 (2009).
6. Z. Zhang and M. Qiu, "Small-volume waveguide-section high Q microcavities in 2D photonic crystal slabs," Opt. Express **12**, 3988 (2004).
7. S. Combrié, A. de Rossi, Q. V. Tran, and H. Benisty, "GaAs photonic crystal cavity with ultrahigh Q: microwatt nonlinearity at 155 μm," Opt. Lett. **33**, 1908 (2008).
8. S. Combrié, Q. V. Tran, A. de Rossi, C. Husko, and P. Colman, "High quality GaInP nonlinear photonic crystals with minimized nonlinear absorption," Appl. Phys. Lett. **95**, 221108–4 (2009).
9. Z. Han, X. Checoury, L.-D. Haret, and P. Boucaud, "High quality factor in a two-dimensional photonic crystal cavity on silicon-on-insulator," Opt. Lett. **36**, 1749–1751 (2011).
10. S. Buckley, M. Radulaski, J. Petykiewicz, K. G. Lagoudakis, J.-H. Kang, M. Brongersma, K. Biermann, and J. Vučković, "Second-Harmonic Generation in GaAs Photonic Crystal Cavities in (111)B and (001) Crystal Orientations," ACS Photonics **1**, 516–523 (2014).
11. H. S. Lee, S. Kiravittaya, S. Kumar, J. D. Plumhof, L. Balet, L. H. Li, M. Francardi, A. Gerardino, A. Fiore, A. Rastelli, and O. G. Schmidt, "Local tuning of photonic crystal nanocavity modes by laser-assisted oxidation," Appl. Phys. Lett. **95**, 191109 (2009).

#313026 https://doi.org/10.1364/OE.26.006400
Journal © 2018 Received 8 Nov 2017; revised 25 Dec 2017; accepted 30 Dec 2017; published 2 Mar 2018

Optics EXPRESS

12. G. Moille, S. Combrié, L. Morgenroth, G. Lehoucq, F. Neuilly, B. Hu, D. Decoster, and A. de Rossi, "Integrated all-optical switch with 10 ps time resolution enabled by ALD," Laser Photon. Rev **10**, 409–419 (2016).
13. Y. Akahane, T. Asano, B.-S. Song, and S. Noda, "High-Q photonic nanocavity in a two-dimensional photonic crystal," Nature **425**, 944–947 (2003).
14. N.-V.-Q. Tran, S. Combrié, and A. de Rossi, "Directive emission from high- Q photonic crystal cavities through band folding," Phys. Rev. B **79**, 041101 (2009).
15. Q. V. Tran, S. Combrié, P. Colman, and A. de Rossi, "Photonic crystal membrane waveguides with low insertion losses," Appl. Phys. Lett. **95**, 061105 (2009).
16. R. W. Boyd, *Nonlinear Optics* (Academic Press, 2013).
17. J. Sipe, D. Moss, and H. van Driel, "Phenomenological theory of optical second- and third-harmonic generation from cubic centrosymmetric crystals," Phys. Rev. B **35**, 1129–1141 (1987).
18. D. E. Aspnes, S. M. Kelso, R. A. Logan, and R. Bhat, "Optical properties of AlxGa1-x As," J. Appl. Phys. **60**, 754–767 (1986).
19. G. Jellison, "Optical functions of gaas, gap, and ge determined by two-channel polarization modulation ellipsometry," Opt. Mater. **1**, 151 – 160 (1992).
20. C. Manolatou, M. J. Khan, S. Fan, P. R. Villeneuve, H. A. Haus, and J. D. Joannopoulos, "Coupling of modes analysis of resonant channel add-drop filters," IEEE J. Quantum Electron. **35**, 1322–1331 (1999).
21. K. Rivoire, Z. Lin, F. Hatami, W. T. Masselink, and J. Vučković, "Second harmonic generation in gallium phosphide photonic crystal nanocavities with ultralow continuous wave pump power," Opt. Express **17**, 22609 (2009).
22. P. S. Kuo, J. Bravo-Abad, and G. S. Solomon, "Second-harmonic generation using -quasi-phasematching in a GaAs whispering-gallery-mode microcavity," Nat. Commun. **5**, 1–7 (2014).
23. M. Galli, D. Gerace, K. Welna, T. F. Krauss, L. O'Faolain, G. Guizzetti, and L. C. Andreani, "Low-power continuous-wave generation of visible harmonics in silicon photonic crystal nanocavities," Opt. Express **18**, 26613 (2010).
24. J. Fürst, D. Strekalov, D. Elser, M. Lassen, U. L. Andersen, C. Marquardt, and G. Leuchs, "Naturally phase-matched second-harmonic generation in a whispering-gallery-mode resonator," Phys. Rev. Lett. **104**, 153901 (2010).
25. M. Fukuda and K. Takahei, "Optically enhanced oxidation of III-V compound semiconductors," J. Appl. Phys. **57**, 129–7 (1985).
26. S. A. Schafer and S. A. Lyon, "Optically enhanced oxidation of semiconductors," J. Vac. Sci. Technol. **19**, 494–5 (1981).
27. F. Intonti, N. Caselli, S. Vignolini, F. Riboli, S. Kumar, A. Rastelli, O. G. Schmidt, M. Francardi, A. Gerardino, L. Balet, L. H. Li, A. Fiore, and M. Gurioli, "Mode tuning of photonic crystal nanocavities by photoinduced non-thermal oxidation," Appl. Phys. Lett. **100**, 033116–5 (2012).
28. C. F. Yu, M. T. Schmidt, D. V. Podlesnik, and R. M. Osgood Jr, "Wavelength dependence of optically induced oxidation of GaAs(100)," J. Vac. Sci. Technol. B **5**, 1087–6 (1987).
29. Z. Lu, M. T. Schmidt, D. V. Podlesnik, C. F. Yu, and R. M. Osgood, "Ultraviolet-light-induced oxide formation on GaAs surfaces," J. Chem. Phys. **93**, 7951–12 (1990).
30. W. G. Petro, I. Hino, S. Eglash, I. Lindau, C. Y. Su, and W. E. Spicer, "Effect of low-intensity laser radiation during oxidation of the GaAs(110) surface," J. Vac. Sci. Technol. **21**, 405–5 (1982).
31. D. D. Nolte, "Surface recombination, free-carrier saturation, and dangling bonds in InP and GaAs," Solid-State Electron. **33**, 295–298 (1990).
32. S. Gehrsitz, F. K. Reinhart, C. Gourgon, N. Herres, A. Vonlanthen, and H. Sigg, "The refractive index of Al[sub x]Ga[sub 1−x]As below the band gap: Accurate determination and empirical modeling," J. Appl. Phys **87**, 7825–14 (2000).
33. F. G. Della Corte, G. Cocorullo, M. Iodice, and I. Rendina, "Temperature dependence of the thermo-optic coefficient of InP, GaAs, and SiC from room temperature to 600 K at the wavelength of 1.5 μm," Appl. Phys. Lett. **77**, 1614 (2000).
34. Y. Zeng, I. Roland, X. Checoury, Z. Han, M. El Kurdi, S. Sauvage, B. Gayral, C. Brimont, T. Guillet, M. Mexis, F. Semond, and P. Boucaud, "Resonant second harmonic generation in a gallium nitride two-dimensional photonic crystal on silicon," Appl. Phys. Lett. **106**, 081105–5 (2015).
35. S. Sokolov, J. Lian, E. Yüce, S. Combrié, A. D. Rossi, and A. P. Mosk, "Tuning out disorder-induced localization in nanophotonic cavity arrays," Opt. Express **25**, 4598–4606 (2017).

1. Introduction

Non-linear optics and, in particular, frequency conversion gained in interest in the past few years. For instance, second harmonic generation (SHG) is used to obtain the beating of the f-2f configuration of a frequency comb [1, 2] while third harmonic generation (THG) is attractive for the high spatial resolution imaging [3, 4] or generation of light at visible wavelength [5]. The required large power densities are easily achieved in small cavities, owing to the resonant enhancement. In this context, III-V semiconductor compounds photonic crystal (PhC) cavities,

Optics EXPRESS

thanks to their small modal volume [6] and the high Q-factor [7–9], are particularly attractive. Interestingly, gallium arsenide (GaAs) was already demonstrated to be a material of choice for resonant SHG operation in PhC cavities providing a large conversion efficiency [10]. However, for large input power and thus large optical power density inside the microcavities, resonators made of GaAs undergo photo-induced oxidation, blue-drifting the resonance wavelength irreversibly. This oxidation process is thermally activated and follows an exponential dependence with the device temperature [11].

In this article, we demonstrate non-linear effects in GaAs PhC cavity, namely SHG and THG with high power density at telecom wavelengths without degrading the device. Indeed, GaAs photo-induced oxidation under large optical power density is quenched thanks to the conformal encapsulation of the GaAs PhC with atomic layer deposition technique where Al_2O_3 surrounds the self-suspended membrane, where the system reaches a local temperature up to about 430 K.

2. Results and discussion

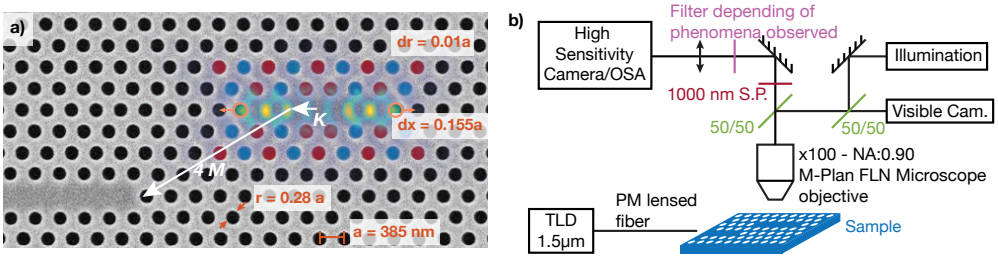

Fig. 1. (a) SEM image of the L_5 PhC cavity. The extractor super-period surrounding the cavity is highlighted, in red for a positive radius variation, in blue for a negative one. The superimposed colored image corresponds to 1508 nm resonant optical spatial mode computed by FDTD – (b) Experimental setup schematic. TLD: Tunable Laser Diode, PM: Polarization Maintained, SP: Short Pass filter, OSA: Optical Spectral Analyzer.

The device here investigated is made of a 250 nm thick GaAs self-suspended membrane grown by metalorganic chemical vapor deposition (MOCVD). The PhC, made of a triangular lattice defined by the vector $\boldsymbol{K} = a\boldsymbol{x}$ and $\boldsymbol{M} = a/2\boldsymbol{x} + a\sqrt{3}/2\boldsymbol{y}$, is patterned using electronic lithography with a period $a = 385$ nm and a hole radius $r = 0.28a$, then transferred to the semiconductor slab through silica hard mask using consecutively a CHF_3–O_2 Reactive Ion Etching (RIE) and $SiCl_4$ inductive coupled plasma (ICP) etching. The membrane is released by selectively etching the sacrificial layer of GaInP below the GaAs slab with a HCl–H_3PO_4 wet etch. The last fabrication step consists of a conformal encapsulation with a 30 nm Al_2O_3 layer deposited by atomic layer deposition (ALD) with in-situ surface pre-treatment consisting of a hydrogen plasma [12]. It was recently shown that such encapsulation and passivation technique helps to reduce the carrier surface recombination velocity [12] The resonator consists of a 5 missing holes cavity, so-called L_5 cavity [13]. The two extrema holes are moved by $dx = \pm 0.155\boldsymbol{K}$ outward from the cavity (Fig. 1(a)) to improve the intrinsic Q factor. A modulation of the hole radii with an amplitude $dr = 0.01a$ is applied in the $\boldsymbol{M}$ directions, corresponding of twice the periodicity of the PhC. This leads to a vertical light extraction [14].

The resonator is connected to an input PhC waveguide with a width $W = 1.05a\sqrt{3}$ at a distance $\boldsymbol{D} = -4\boldsymbol{M} - \boldsymbol{K}$ from the center of the cavity (Fig. 1(a)). The end of the waveguide is composed of an inverted tapers [15] reducing insertion losses from lensed fiber and avoiding Fabry-Perot interferences.

The cavity resonance is measured with a CW tunable laser (Santec) by detecting the direct upward transmission (Fig. 1(b)). We find experimentally a resonance wavelength for the second

Optics EXPRESS

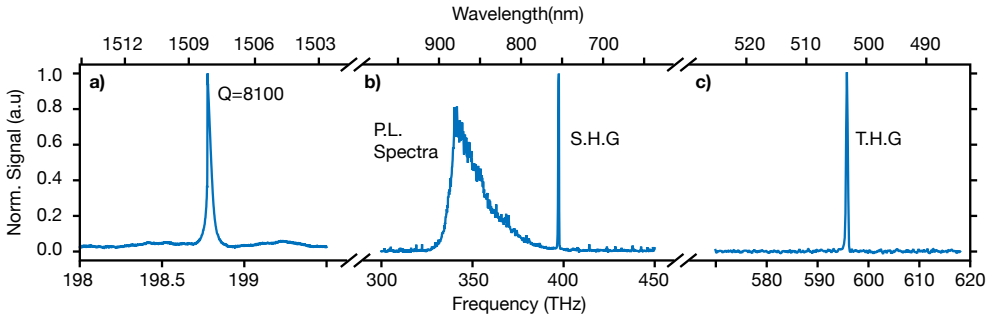

Fig. 2. Spectra of (a) the cavity resonance at telecom wavelength – (b) second harmonic generation and photo-luminescence – (c) third harmonic generation. a) is measured through the transmission of the device at low input power, (b) and (c) are measured with an optical spectrometer

order mode at 1508.2 nm with a Q factor of $Q = 8100$ (Fig. 2(a)). The SH (Fig. 2(b)) and TH signals (Fig. 2(c)) are spectrally characterized using Optical Spectral Analyzers (OSA, Thorlabs, and Ocean Optics respectively), and the signal peaks lie at 754.1 nm and 502.75 nm respectively. Interestingly, the photo-luminescence (PL) can be easily detected as the excitation at 1508 nm leads to two-photon absorption, and the PL signal is spectrally separated enough from the SH one. Therefore both can be independently characterized.

Mode profiles of the SH and TH signals are observed using the setup shown in Fig. 1(b). The light is collected using a microscope objective (Olympus-M plan) with a large Numerical Aperture $NA = 0.9$ and a magnification of 100. The image is observed thanks to a high sensitivity cooled-down EMCCD camera (Andor) with a 512×512 pixels matrix. Each pixel has a size of 16 µm. The effective resolution obtained is 72 nm by pixel (*i.e.* magnification of 220). Appropriate filters are inserted in the setup to observe only the SHG or the THG (band pass filters). The resulting images are shown respectively in Fig 3(a) and (c).

Theoretical SH and TH mode profiles are retrieved by modeling the optical spatial mode distribution at the resonance wavelength and by computing the induced polarization [16, 17] using an in-house developed 3D-FDTD code (Fig. 3(b) and (d)). In order to compare fairly the experiment with the modeling, those last results are convoluted with the numerical aperture of the microscope objective, and the absorption length is taken into account in the simulations (*i.e.* 570 nm for SH signal and 110 nm for TH signal). The simulation results are in good agreement with the measurements, although for the induced polarization at the SH wavelength, the differences between the modeling and the characterized profile are more noticeable. This could be explained by the optical index (both real and imaginary part) which could tend to differ from the value found in the literature for $\lambda = 754.1$ nm [18, 19] due to the optical pumping and two photon-absorption at 1.5 µm.

It is highly interesting to note that resolving the TH spatial mode allows one to resolve the resonant mode at telecom wavelength. Indeed, as previous work pointed out [4], the spatial distribution of the THG is proportional to E^3_{pmp}. Thanks to the diffraction limit greatly reduced using the TH signal as compared to the telecom one and thanks to the the short absorption length (110 nm) avoiding light propagation in the structure, the measured mode at 502 nm is close to the resonant pumped mode profile at 1508 nm.

The conversion efficiency of both SH and TH were characterized. Due to thermal effect, mostly induced by carrier recombination, the input CW signal is tuned for each input power to match the shifted resonance. Using the same setup previously shown in Fig. 1, it allows us to measure the output signal power. Indeed, the photons are counted using the EMCCD camera, thus the

Optics EXPRESS

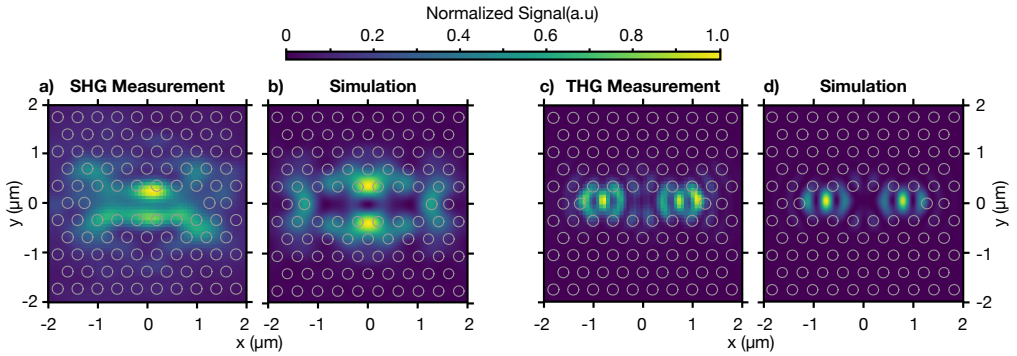

Fig. 3. (a) SH mode profile measured – (b) Induced polarization at SH wavelength from mode profile at the cavity resonance computed with FDTD – (c) TH mode profile measured – (d) Induced polarization at TH wavelength from modeling

Table 1. Summary of the different losses in the optical detection path for SH and TH wavelengths.

Element	**Losses (754.1 nm)**	**Losses (502.75 nm)**
Microscope obj.	-0.71 dB	-0.97 dB
50/50 mirror	-3 dB	-3 dB
1000 nm S.P. filter	-0.08 dB	-0.13 dB
End filter	-1.08 dB	-1.31 dB

detected power. Here, only the area corresponding to the cavity is accounted. A normalization is performed taking into account all the different losses at the SH and TH wavelength (Table 1) leading to a total collection losses of −4.87 dB for the SH and −5.41 dB for TH signal. The insertion losses of the waveguide are estimated to be -7 dB. Thus, the total efficiency conversion for the SHG operation found is $P_{SHG}/P_{in}^2 = 8.3 \times 10^{-5}$ W^{-1}, while for the THG conversion is $P_{THG}/P_{in}^2 = 1.2 \times 10^{-3}$ W^{-2} (Fig. 4). Saturation effects appear at high input power, mostly due to two-photon absorption and free-carrier absorption [12], which is predicted by the Coupled Mode Theory (CMT) [20].

These values are still below the state of the art of SHG and THG for nano-structured system [10,21–23]. However, the conformal encapsulation of the system prevents photo-oxidation, and high input power are achievable without any material degradation. This leads to a second harmonic generation of 0.2 nW, orders of magnitude larger than in ref. [10]. This value is close to the record of SHG observed in other III-V materials PhC cavities [21] and order of magnitude higher than previous work on GaAs [10] or Silicon [23] PhC cavities (*i.e.* non-resonant at SH wavelength). SHG powers could be enhanced owing to resonant SH, design achievable using, for instance, micro-disk [24]. Nevertheless, photo-induced oxidation was observed in our different uncoated sample and in the literature, mostly resulting from free carrier generation/recombination [25,26]. This leads to an irreversibly blue shift of the resonance. Owing to the conformal encapsulation of the material through the ALD technique, no change in the resonance wavelength was observed, thus no photo-oxidation process.

We now address the stability over input power as it is one of the main key aspect for efficient SHG and THG. Indeed, GaAs undergoes photo-induced oxidation. A variety of processes results into enhanced oxidation such as thermally induced [11, 25], catalytic effect of electron-hole pairs [27], hot carrier for efficient O_2 adsorption [28, 29]. All those effects are directly linked

Optics EXPRESS

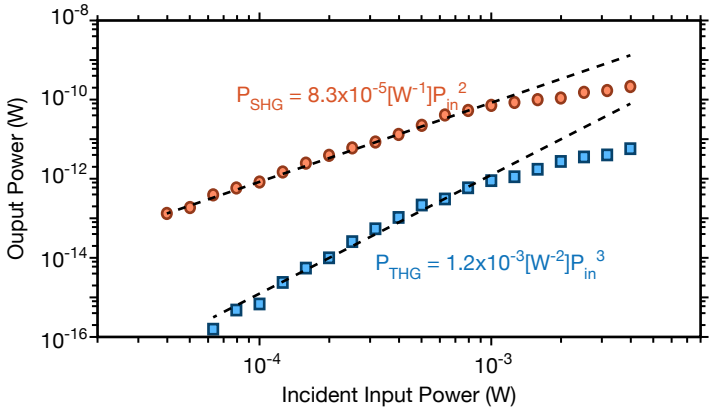

Fig. 4. Second (red circles) and third harmonic generation (blue squares) power level versus input coupled power. The dashed lines correspond of a quadratic and cubic fit of SHG and THG respectively and from which conversion efficiency is extracted.

with O_2 adsorption on the GaAs surface. In regards with the Telecom wavelength here, which generates carriers through two-photon absorption (TPA) just above the band-gap, the main oxidation effect is the thermally induced one through carrier recombination [30], and enhanced by the high carrier surface recombination velocity [12, 31]. Therefore, we will focus on the later.

To investigate further the oxidation process, we look at the temperature of the resonator, using two main different techniques. First by observing the modification of the photo-luminescence spectra (Fig. 5(d)) using an OSA (Thorlabs), the band gap energy can be probed. Thus one can retrieve the material temperature as the peak of the photo-luminescence minus $k_B T/2$ is directly linked to the temperature [32]. Secondly the spectral shift of the resonance, measured by probing the THG (Fig. 5(c)), SHG (Fig. 5(b)) and the direct transmission at 1.5 µm (Fig. 5(a)), allows one to measure the shift of the refractive index, hence the temperature of the cavity [33]:

$$n = -1.86 \times 10^{-10} \frac{T^3}{3}[\mathrm{K}^{-3}] + 3.49 \times 10^{-7}[\mathrm{K}^{-2}]\frac{T^2}{2} + 1.47 \times 10^{-4}[\mathrm{K}^{-1}]T + 3.431869 \quad (1)$$

Using FDTD computation, the resonance wavelength dependence with the refractive index of this specific device can be retrieved. Considering the equation above, it is easier to write the dependence of the resonance wavelength versus the refractive index:

$$\lambda = 5.1 \times 10^{-8}[\mathrm{m}]n^2 + 5.7 \times 10^{-8}[\mathrm{m}]n + 6.881[\mathrm{m}] \times 10^{-7} \quad (2)$$

Fig 5(e) exhibits the coherence of the results through the four measurements made at room temperature, and mostly the consistency of the results through the two main types of characterization. A small wavelength detuning is measured in the transmission map between direct transmission compared to SHG and THG, which was already observed in other nitride based material [34]. The maximum increase of the sample temperature is of about 130 K, namely a resonator temperature of about 430 K which last during several minutes. Even after few experiments reaching this temperature, no modifications are observed in the cold resonance wavelength, namely after the cavity has cooled down to room temperature.

In comparison, previous works shown that for an uncoated GaAs sample and a heating at a temperature of 434 K during 3 min, the PhC resonator exhibited, after cooling down, a resonance spectral blue shift of 1.4 nm from the resonance at room temperature. Thermally activated oxide thickness, therefore the irreversible blue wavelength shift [11], can be described by $\Delta\lambda_{res} \propto \sqrt{D_O} \exp\left(\frac{E_a}{2k_B T}\right)\sqrt{t}$, where D_O is the diffusivity of oxygen in the material and E_a

Optics EXPRESS

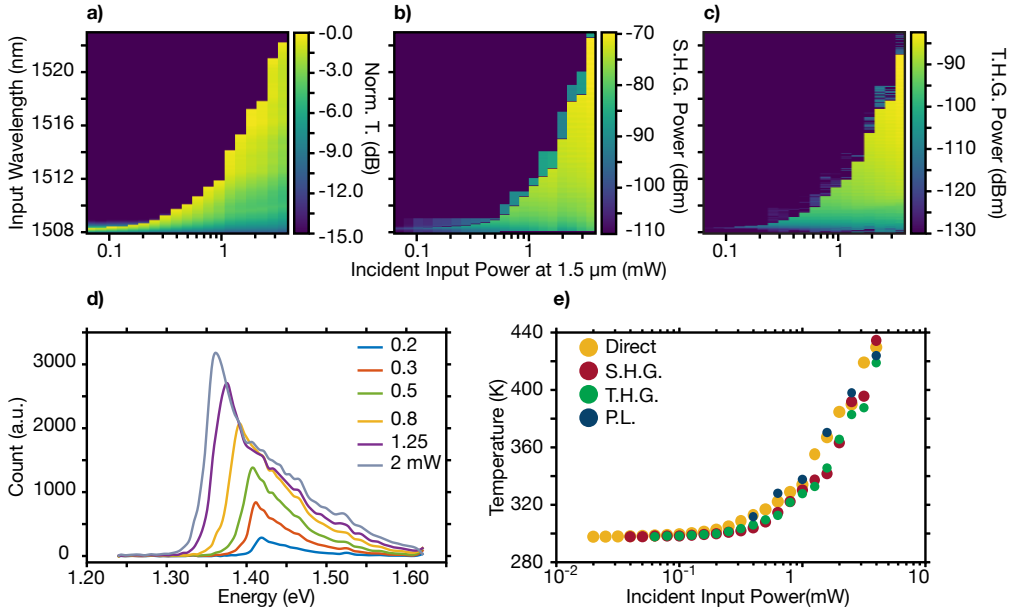

Fig. 5. Measurement of the transmission (colormap) of (a) direct transmission at 1.5 μm (b) SHG signal and (c) THG signal versus the input power and the input wavelength. (d) Measurement of the photoluminescence for different input power at 1.5 μm. (e) Extracted temperature of the cavity using the two methods, namely spectral shift (blue, red and green circles) and band-gap energy measurement (yellow circles)

the activation energy. Our total experimental time is order of magnitude longer than the one shown in ref. [11] (experiments shown here are on the time scale of several minutes for the same input power, and have been repeated several time), without exhibiting any irreversible change in the resonance wavelength. We can then conclude that the ALD layer creates a barrier from the atmosphere, reducing drastically the diffusivity of oxygen into the GaAs, and then quenching photo-induced oxidation. It allows to reach high input power, thus high SH and TH output power.

3. Conclusion

In conclusion, we have shown here high output power for SHG and THG in PhC resonator made of GaAs. Indeed, conform encapsulation of the material with Al_2O_3 made by ALD prevents photo-induced oxidation leading to an irreversible blue shift of the resonance. Therefore, high input power can be injected into the system without permanently damaging the structure. Measurement of the system temperature was achieved by measuring the shift of the resonance wavelength and by measuring the photo-luminescence spectra. The system reaches a maximum temperature of 434 K, without any degradation of the resonator. This open new perspectives such as, thermally controlling the cavity resonance [35] without degrading the material or, the improvement of SHG and THG power collected in integrated micro-cavities.

Funding

Agence Nationale de la Recherche (ETHAN, ANR-15-ASTR-0014; AUCTOPUSS,ANR-12-ASTR-0014).